

Synthesis, Characterization, and Crystal Structures of 1,1-Disubstituted-2,3,4,5-tetraphenylgermoles That Exhibit Aggregation-Induced Emission

Teresa L. Bandrowsky, James B. Carroll, and Janet Braddock-Wilking*

Department of Chemistry and Biochemistry and Center for Nanoscience, University of Missouri—St Louis, St. Louis, Missouri 63121, United States

S Supporting Information

ABSTRACT: A series of 2,3,4,5-tetraphenylgermoles with different 1,1-substituents have been prepared, and their UV–vis absorption and fluorescence spectral profiles in solution were determined. A thin-layer chromatography based method was used to measure their solid-state luminescence. Nine of the 11 new germoles have been characterized crystallographically. The aggregation-induced emission effect in these germoles was studied, and significant enhancement of the photoluminescence and quantum yield in mixed solvent–water systems was determined. Scanning and transmission electron microscopy analysis revealed the formation of nanocrystalline aggregates in the mixed solvent–water systems and after exposure of the germoles to acetone, a volatile organic chemical.



INTRODUCTION

Silacyclopentadienes, or siloles (Figure 1), are a class of molecules that have been extensively developed for their potential application in organic electronics, particularly in flexible lighting and display panels.¹ One of the qualities responsible for the intense interest in siloles is the high electron affinity that these cyclic molecules exhibit.² Such large electron affinities can be attributed to a low-lying LUMO, which arises from $\sigma^*-\pi^*$ conjugation that results from the interaction between the π^* orbital of the butadiene segment and the σ^* orbital associated with the two exocyclic bonds on the silicon center.³ The large electron affinity of the siloles results in another favorable feature, high electron mobility,⁴ a desirable attribute that continues to present challenges in the design of highly efficient organic electronic devices. There are many silole derivatives that have been reported to be good electron transporters with electron mobilities that are 2 orders of magnitude higher than tris-(8-hydroxyquinolato)aluminum (Alq₃).^{4,6a} Alq₃ is a commonly used electron-transport (ET) material for organic light-emitting diodes (OLEDs).⁵

Siloles have demonstrated high photoluminescence (PL) quantum yields as both amorphous and crystalline solids, which can be attributed to the unique photophysical property of aggregation-induced emission (AIE).⁶ As a result of the steric repulsions between the peripheral aryl substituents on the core ring, intramolecular rotations of the substituents are restricted, causing the substituents on the silole core to assume a highly twisted conformation that persists in solution as well as the solid state. Restriction of intramolecular rotations of the peripheral substituents effectively blocks nonradiative relaxation channels and imparts nonplanarity, rendering the distance between adjacent

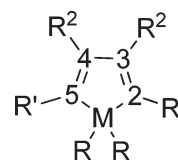


Figure 1. Basic metallole structure. M = Si, silole; M = Ge, ger mole; 2, 3, 4, 5 = C.

silole molecules too long for conventional $\pi-\pi$ stacking interactions ($\sim 3-4 \text{ \AA}$)¹ that typically quench luminogens in the solid and crystalline phases. This mechanism is referred to as restricted intramolecular rotation (RIR) and is the accepted cause of the AIE phenomenon.^{7,8} RIR so effectively deactivates the avenues that result in nonradiative emission that siloles strongly emit light in the solid and crystalline phases, such as aggregated suspensions in solvent–water mixtures.

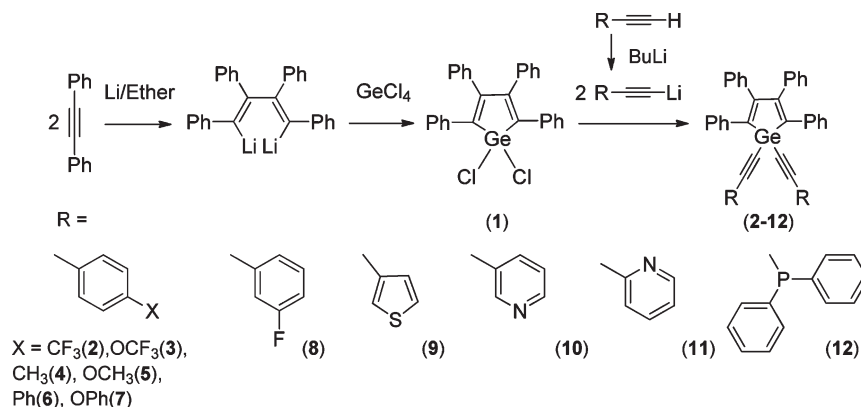
The AIE effect has now been identified in other luminogens with similar structural features including ger moles,⁹ the heavier group 14 congener of siloles. Although ger moles emit more efficiently in solution than siloles,⁸ their solutions are still only weakly emissive.⁹ The increased efficiency in solution, however, does not diminish the significant AIE effect that is exhibited by ger moles in the solid state or when aggregated in solvent–water mixtures. Ger moles, like siloles, are soluble in a variety of common organic solvents, but insoluble in water.

To date, relatively little has been published on the photoluminescence of ger moles, despite published evidence of the

Received: March 24, 2011

Published: June 09, 2011

Scheme 1



similarities between siloles and germoles. In addition to exhibiting the AIE effect, parallels between the electronic structure and photophysical properties of the two metalloles can be seen by the similarities in the UV–vis absorption and fluorescence profiles,¹⁰ electrochemical data, and ab initio calculations of HOMO and LUMO energy levels.¹¹ Such studies indicate comparable σ^* (Si–R) and σ^* (Ge–R) orbitals as well as low-lying LUMO energy levels, suggesting that the differences in the electronic structures of germanium and silicon analogues are relatively minimal despite the slightly larger size of the germanium atom. This is in contrast to the attributes that would be gleaned from the low-lying LUMO in stannoles, which are diminished by significantly less efficient $\sigma^*-\pi^*$ conjugation that results from a greater orbital mismatch as well as elongated bond distances between the larger $5p_z$ σ^* orbital of tin and the $2p_z$ π^* orbital of the carbons of the butadiene.^{10,12} We now report the synthesis and characterization of a series of new 2,3,4,5-tetraphenylgermoles with different 1,1-substituents and the experimental data describing the AIE effect in these germoles. Scanning electron microscopy (SEM) and transmission electron microscopy (TEM) images are presented to indicate the nature of the aggregate formation within these germoles.

RESULTS AND DISCUSSION

Synthesis. 1,1-Dichloro-2,3,4,5-tetraphenylgermole (**1**) was prepared by a ring-closure reaction of 1,4-dilithio-1,2,3,4-tetraphenyl-1,3-butadiene with germanium tetrachloride according to the procedure reported by Curtis.¹³ In contrast to the synthesis of 1,1-dichloro-2,3,4,5-tetraphenylsilole,¹⁴ the germole can be prepared without difficulty in high yield (70–95%). Isolated **1** was converted to new 1,1-disubstituted germoles (**2** through **12**) by addition of various alkynyllithium reagents that had been generated from commercially available terminal acetylenes and ⁿBuLi (Scheme 1). Due to the relatively short lifetime of the lithiated alkyne species,¹⁵ the yields of germoles **2** through **12** were lower and varied from 44% to 70%. The diphenylphosphine-substituted precursor is not commercially available and was prepared according to a known procedure.¹⁶ The new germoles were characterized by multinuclear NMR spectroscopy, elemental analyses, X-ray crystallography, and UV–vis and fluorescence spectroscopy. NMR resonances and couplings exhibited by germoles **2–12** were within expected values.

Table 1. Crystallographic Data and Structure Refinement for **8** and **12**

	8	12
formula	C ₄₄ H ₂₈ F ₂ Ge	C ₅₆ H ₄₀ GeP ₂
fw	667.29	847.41
cryst size/mm	0.32 × 0.33 × 0.38	0.40 × 0.60 × 0.80
cryst syst	triclinic	triclinic
space group	P $\bar{1}$	P $\bar{1}$
a/Å	10.555(2)	11.4828(14)
b/Å	11.095(2)	12.9012(13)
c/Å	15.680(3)	18.022(2)
α /deg	92.23(3)	71.258(3)
β /deg	104.77(3)	77.857(4)
γ /deg	113.52(3)	64.911(4)
V/Å ³	1607.5(8)	2281.2(4)
D _{calcd} /g cm ⁻³	1.379	1.234
Z	2	2
abs coeff/mm ⁻¹	0.996	0.778
θ range/deg	1.36 to 34.02	1.20 to 24.99
reflns collected/indep reflns	50 264/12 224	22 480/7943
	[R(int) = 0.027]	[R(int) = 0.041]
abs correct	numerical	numerical
max. and min. transmn	0.7467 and 0.6576	1.000 and 0.8625
final R indices [$I > 2\sigma(I)$]	0.0395	0.0390
R indices (all data)	0.1121	0.1310

X-ray Crystal Structures. Single crystals of the germoles were grown from a variety of solvent mixtures, which are noted in the Experimental Section, as fluorescent greenish-yellow blocks. X-ray quality crystals were obtained for all of the new germoles with the exception of **3** and **6**, due to the problems encountered in the recrystallization attempts and inability to refine the data adequately, respectively. Germole **5** crystallized as the tetrahydrofuran solvate. Generally, the structure refinement proceeded according to acceptable models with reasonable parameter discrepancies and residual electron densities. Table 1 contains the crystallographic data for **8** and **12**. A summary of the crystal data and intensity parameters for all of the remaining crystal structures that were obtained is provided in the Supporting Information.

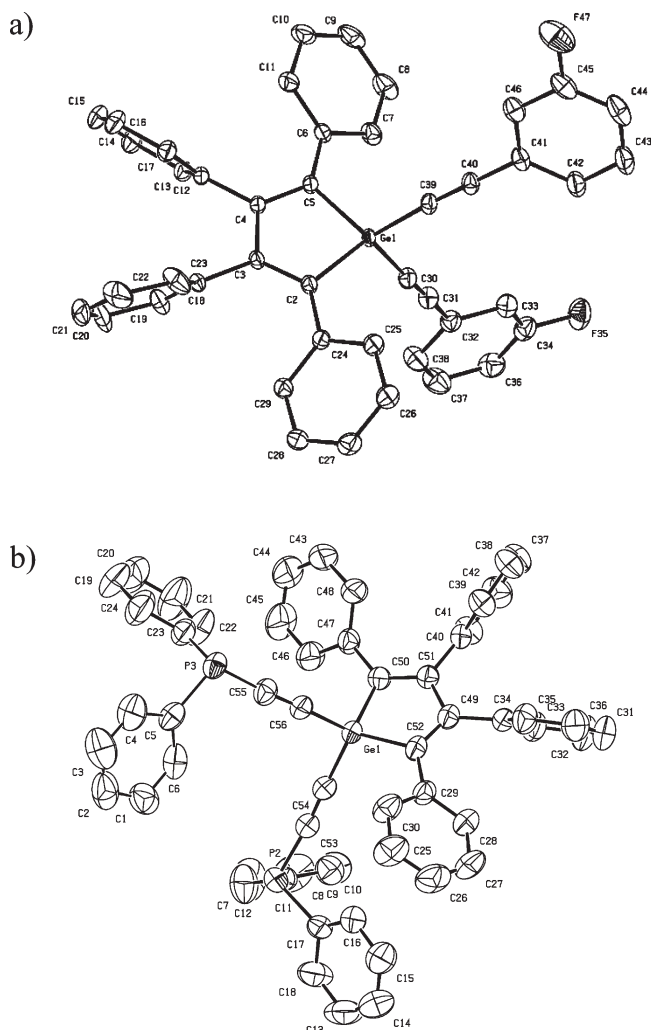


Figure 2. (a) Selected bond distances (Å), angles (deg), and torsions (deg) for **8**. Thermal ellipsoids are shown at the 50% probability level: Ge1–C30 = 1.890(2), Ge1–C39 = 1.897(2), Ge1–C2 = 1.954(1), Ge1–C5 = 1.940(2), C2–C3 = 1.362(2), C3–C4 = 1.512(2); C2–Ge1–C5 = 91.83(6), Ge1–C2–C3 = 106.2(1), Ge1–C5–C4 = 105.8(1), C2–C3–C4 = 117.5(1), C3–C4–C5 = 118.6(1), C30–Ge1–C39 = 105.68(7); Ge1–C2–C24–C25 = 36.5(2), Ge1–C5–C6–C7 = 30.3(2), C2–C3–C18–C19 = –113.9(2), C5–C4–C12–C13 = 61.8(2). (b) Selected bond distances (Å), angles (deg), and torsions (deg) for **12**. Thermal ellipsoids are shown at the 50% probability level, and the hydrogen atoms and the disorder on **12** have been omitted for clarity: Ge1–C50 = 1.929(2), Ge1–C52 = 1.940(3), C49–C51 = 1.516(4), C50–C51 = 1.349(4), Ge1–C54 = 1.897(4), Ge1–C56 = 1.904(4), P2–C53 = 1.774(4), P3–C55 = 1.74(1); C50–Ge1–C52 = 91.5(1), Ge1–C50–C51 = 106.6(2), C50–C51–C49 = 117.9(3), C51–C49–C52 = 117.3(3), C54–Ge1–C56 = 105.5(1); Ge1–C50–C47–C46 = –48.7(4), Ge1–C52–C29–C30 = –35.7(4), C52–C49–C34–C35 = –56.7(5).

The molecular structures of **8** and **12** are shown in Figure 2 and are representative of all of the germoles described in this study. Selected bond lengths and angles listed in Figure 2 illustrate the general agreement of the geometric parameters for **2**, **4**, **5**, and **7–12**. A search of the Cambridge Structural Database exhibited nine entries for germacyclopentadienes.¹⁷ The geometries of **2**, **4**, **5**, and **7–12** matched seven of the nine entries found from the search. The average Ge–C bond length

from the search was 1.933 Å, which is in close agreement to the average bond length of 1.938 Å for the germoles reported herein. The average C=C and C–C bond lengths of the central ring for **2**, **4**, **5**, and **7–12** are 1.357 and 1.511 Å, respectively, which once again correlate well with the CSD data of 1.350 and 1.507 Å. The average Si–C bond length was reported to be 1.869 Å, while the average C=C and C–C bond lengths were 1.363 and 1.494 Å, respectively.¹⁸ The exocyclic Ge–C bond lengths, 1.895 and 1.893 Å, are slightly longer than the reported CSD data of 1.859 and 1.846 Å, which may be due to the steric requirements of the bulky 1,1-substituents. The C2–Ge–C5 bond angle of the central ring for **2**, **4**, **5**, and **7–12** is 91.5°, which is in agreement with the CSD data of 91.3°.

The drawings in Figure 2 illustrate the highly twisted conformation that the phenyl substituents assume relative to the germacyclopentadiene core. The peripheral phenyl substituents on the ring carbons are twisted out of plane with respect to the ring core and are twisted with the same sense within the compound. The average dihedral angle for the phenyl substituents on the 2,5-ring carbons for **2**, **4**, **5**, and **7–12** was ca. 38° and for the 3,4-ring carbons ca. 63°, which is consistent with the reported dihedral angles of ca. 30° and ca. 70° for tetraphenyl-substituted siloles.¹⁹

The only exception was **7**, whereby the germanium lies in a special position and has dihedral angles of 15.7° and 65.3° for the phenyl substituents on the 2,5- and 3,4-ring carbons, respectively. The dihedral angles reported for 1,1-diphenyl-2,3,4,5-tetraphenylgermole for the 2,5-ring carbon substituents were 0.7° and 46.1°, while the 3,4-ring carbon substituents were 96.8° and 63.4°, respectively.^{9d} An analysis of the data obtained from the crystal structures suggests that the dihedral angles of **2**, **4**, **5**, and **7–12** are more similar to those in tetraphenyl-substituted siloles than the other germole derivatives characterized by Tracy et al.^{9c,d} Selected torsion angles for three of the germoles are depicted in Table 2. As a result of these similarities, modifications at the 2,5- and 3,4-positions of these germoles may be related to similar effects on the electronic and optical properties that have been observed in siloles.²⁰

Electronic Transitions. The absorption spectra for solutions of germoles **2–12** in methylene chloride were measured, and the spectral data are summarized in Table 3. All of the germoles **2–12** exhibit an absorption maximum between 364 and 369 nm. Germoles **2–12** weakly emit in the region of 478–488 nm in solution at room temperature with quantum yields that range from 0.0046 to 0.0071. Under similar experimental conditions, germoles **2–12** exhibited quantum yields ca. 3× greater than either 1,1-dimethyl- or 1,1-diphenyl-2,3,4,5-tetraphenylgermole, for which the reported quantum yields were 0.0015 and 0.0026, respectively.^{9d}

Consistent with the trend observed for siloles, manipulations of the 1,1-substituents imposed a similar shift to longer absorption maxima as the substituents directly attached to the germanium center increased in electronegativity.²¹ Among a series of germoles possessing the same 1,1-substituents, the UV absorption maxima red shift in the order of Me (350 nm) < Ph (358 nm) < C≡CH (362 nm) < C≡C–R (364–369 nm for **2–12**).^{9a,d}

Substitutions on the β-position of the triple bond (the terminal position of the alkyne) also reflected a modest red shift as more electronegative groups were introduced. The upper and lower range of the absorption maxima are illustrated by Figure 3. This is in contrast to silole derivatives possessing alkynyl substituents at the 1,1-positions, where the absorption and

Table 2. Selected Torsion Angles (Degrees) of 8, 9, and 11

phenyl substituent attached to ring carbon	8	9	11
C1	Ge1–C14–C15–C16 31.3(3)	Ge1–C2–C24–C25 33.4(2)	Ge1–C31–C17–C35 –27.3(1)
C2	C14–C13–C21–C22 63.4(3)	C2–C3–C18–C19 59.1(2)	C31–C11–C42–C15 –59.1(1)
C3	C13–C12–C27–C28 68.8(3)	C3–C4–C12–C17 65.4(2)	C11–C30–C19–C37 –65.9(1)
C4	Ge1–C11–C33–C38 36.3(3)	Ge1–C5–C6–C11 42.7(2)	Ge1–C21–C3–C39 –46.6(1)

Table 3. Absorption and Emission Data for 0.01 mM CH₂Cl₂ Solutions of 2–12 at Room Temperature ($\lambda_{\text{ex}} = 370 \text{ nm}$)

germole	absorption λ (nm)	emission λ (nm)	Φ_{F}^a
4	364	480	0.00457
3	365	478	0.00570
5	365	482	0.00464
9	366	485	0.00578
7	366	486	0.00508
6	367	485	0.00569
10	368	487	0.00627
2	369	483	0.00582
8	369	488	0.00538
12	369	487	0.00706
11	369	486	0.00689

^a 9,10-diphenylanthracene was used as a standard.

emission wavelengths remained unchanged despite varying the β -substituents of the alkyne from hydrogens to phenyls.²² Such data suggest a greater sensitivity in germoles to the identity of the substituents, even those that are at more remote bonds from the germanium center and may allow more control in fine-tuning the electronic properties.

Solid-State Photoluminescence. The solid-state photoluminescence was measured using a thin-layer chromatography (TLC) method developed by Tang et al.,²² and the emission wavelengths are summarized in Table 4. The thin layer of all the new germoles absorbed on the TLC plate fluoresce intensely in the blue-green region. The intensity of the PL emission significantly increased compared to the corresponding weakly emissive solutions. The trend in the red shift in the emission wavelengths was not readily apparent; efforts are currently underway to elucidate the nature of the effects when manipulating the 1,1-substituents on the luminescence properties of 2–12 in the solid and crystalline phases. The new germoles exhibited Stokes shifts between 117 and 132 nm. These values are consistent with the reported Stokes shift for siloles, which vary between 120 and 129 nm,²² as well as those reported for 1,1-dimethyl- or 1,1-diphenyl-2,3,4,5-tetraphenylgermole (117 and 130 nm, respectively).^{9d} Stokes shifts greater than 100 nm are necessary for applications that require ultrahigh sensitivity such as fluorescence imaging measurements and bioprobes for protein detection and quantification.²³

Aggregation-Induced Emission. While the AIE effect has been demonstrated in germoles, the availability of germole derivatives is limited, which is why the AIE phenomenon was explored in several of the germoles prepared in this study.

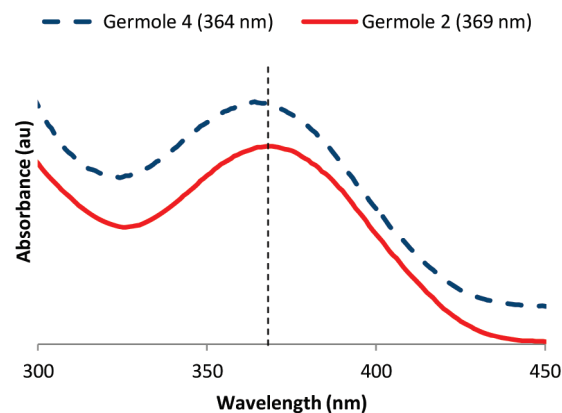


Figure 3. Absorption spectra for the methylene chloride solutions of germoles 2 and 4, which represent the range of the UV absorption maxima.

Germole 2 is soluble in acetone, as verified by dynamic light scattering measurements, but is insoluble in water. Initially 2 was dissolved in pure acetone, and then a specified amount of water was added. Once the water was added to the mixture, the solubility of 2 was reduced, causing aggregation, which resulted in an increase in the photoluminescence. As illustrated by Figure 4, the dilute acetone solution of 2 is weakly emissive; however, as the proportion of water to acetone increased in the mixed solvent system, the photoluminescence significantly increased. A similar increase in photoluminescence upon addition of water to either an acetone or acetonitrile solution of the germole was also observed for 6, 8, 11, and 1,1-diethynyl-2,3,4,5-tetraphenylgermole.²⁴ All variations within the mixed solvent system exhibited similar spectral profiles with minimal shifting of the emission wavelength maximum, which is consistent with similar siloles and germoles.^{6b} Typically, aggregation results in a red shift of the emission wavelength.²⁵ Noteworthy is the indication that the onset of AIE begins at ca. 30% water content within the mixed solvent system, although the phenomenon is modest. Tracy and co-workers studied similar concentrations of 1,1-dimethyl- and 1,1-diphenyl-2,3,4,5-tetraphenylgermole in a variety of mixed solvent–water systems and reported the earliest occurrence of AIE was between 60% and 70% water content in a mixed water–dioxane system.^{9c}

The increase in the PL intensity of 2 correlated with an increase in the emission quantum yield, as shown in Figure 5. The quantum yields in the acetone and acetone–water mixtures were calculated using 9,10-diphenylanthracene as a standard.²⁶ The quantum yield of the acetone solution of 2 was 0.0040.

Table 4. Solid-State Emission Data for 2–12 at Room Temperature ($\lambda_{\text{ex}} = 370$ nm)

germole	emission λ (nm)	Stoke's shift (nm)
6	484	117
3, 4, 7, 9	485	120, 121, 119, 119
2	486	117
11	490	121
5	492	127
8, 12	493	124
10	500	132

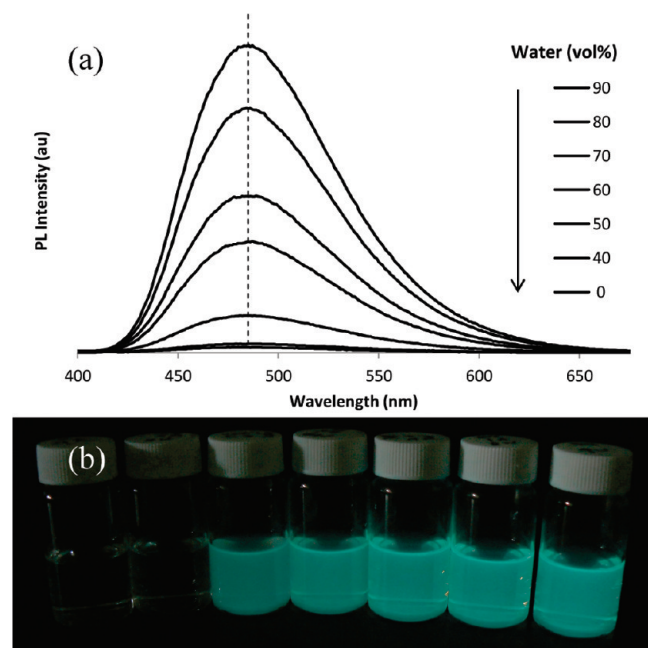


Figure 4. (a) PL spectra for 0.01 mM **2** in pure acetone and acetone–water mixtures at room temperature ($\lambda_{\text{ex}} = 370$ nm); (b) photo of the solutions of **2** in pure acetone (far left) and acetone–water mixtures (40%, 50%, 60%, 70%, 80%, and 90%, respectively), which correlates with the graph of the PL spectra.

A modest increase in the quantum yield to 0.0050 was observed at a water content of ca. 30%, implying that intramolecular motions of **2** were already being minimized. Restriction of the intramolecular motions of **2** resulted in increased PL intensity (the AIE effect), which although not discernible by the naked eye, was detectable with instrumentation. An expanded view of Figure 5 depicting the increase in the quantum yield at the lower water contents is available in the Supporting Information. The increased PL intensity is supported by the increase in quantum yield. When the water content of the acetone–water system was 90%, the quantum yield increased to 0.26, which is 65 times higher than the acetone solution.

All variations within the mixed acetone–water solvent system exhibited a similar absorption spectral profile with broad absorption bands that trail into the long-wavelength region and a slight red shift of the wavelength maximum (Figure 6). The spectral profiles imply that **2** has aggregated in the acetone–water mixtures, as both broad absorption bands and red shifts are characteristic optical responses related to the Mie scattering

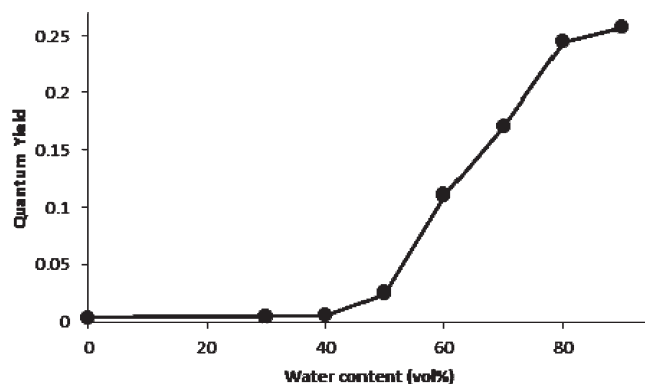


Figure 5. Quantum yield of **2** vs the water content of the mixed acetone–water systems.

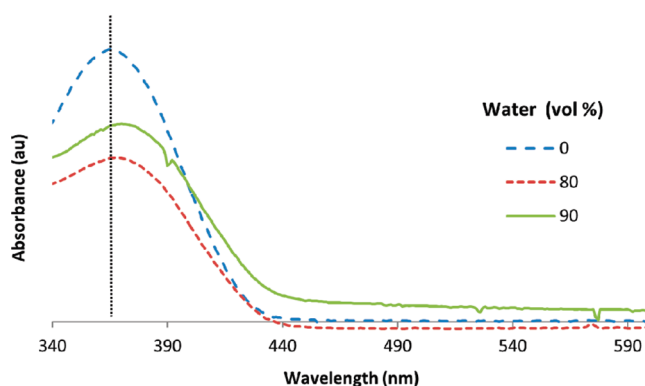


Figure 6. Absorption spectra of 0.01 mM **2** in the mixed acetone–water solvent systems.

effect associated with the presence of small, metallic particles.²⁷ Dynamic light scattering measurements taken within ca. 40 min of preparing the samples also suggest that **2** had aggregated into nanoparticles with average sizes of 47 and 74 nm in the acetone–water mixtures with water contents of 80% and 90%, respectively.

TEM measurements were used to investigate the nature of the aggregate formation in the acetone–water mixtures. In the 10% acetone–90% water mixture, the TEM images of **2** depicted the formation of nanoparticles with individual dimensions that were closer to 100 nm that aggregate in small clusters (Figure 7a). The smaller aggregate clusters were more prevalent than the larger aggregate clusters; an example of one of the larger aggregate clusters is given in Figure 7b.

The crystalline nature of the particles was confirmed by electron diffraction patterns (Figure 7c). As in solid phase crystals, it is reasonable to conclude that the aggregates pack in an arrangement that minimizes π – π stacking of any planar segments of the germole. Lack of intermolecular π – π interactions as well as an increased restriction of any molecular motions imposed by the crystalline lattice would promote the photoluminescence observed in the acetone–water mixtures.

Applications. The germoles, **2**, **8**, and 1,1-diethynyl-2,3,4,5-tetraphenylgermole²⁴ were tested as potential chemosensors for the detection of volatile organic compounds (VOCs) such as acetone. The photoluminescence was monitored as thin films of the germoles that were exposed to acetone vapor. TLC plates

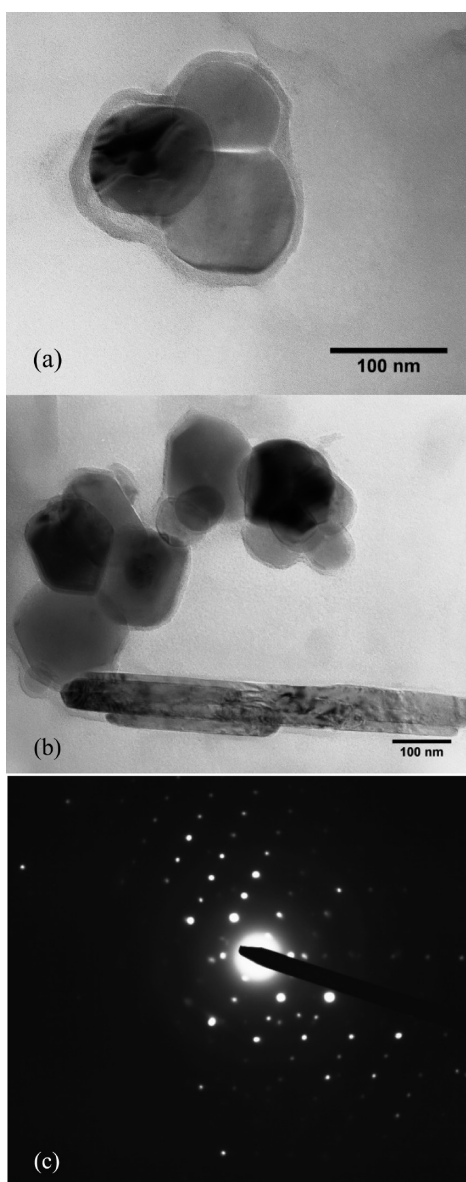


Figure 7. TEM images of **2** illustrating the small aggregate clusters (a) and larger aggregate clusters (b) that were observed in the water–acetone mixture containing 90% water; the electron diffraction pattern (c) exhibited by aggregates in the 10% water–90% acetone mixture.



Figure 8. Photos of the TLC plates of **8** (a) prior to solvent exposure, (b) after exposure, and (c) after the solvent evaporated.

were spotted with $\sim 10^{-3}$ M methylene chloride solutions of the germoles and allowed to thoroughly dry in air. As can be seen in Figure 8a, the thin film of **8** intensely fluoresces. Upon exposure to acetone vapor, the emission is rapidly quenched (Figure 8b). This is consistent with the acetone vapor condensing on the TLC plate and dissolving the germole, which quenches light emission,

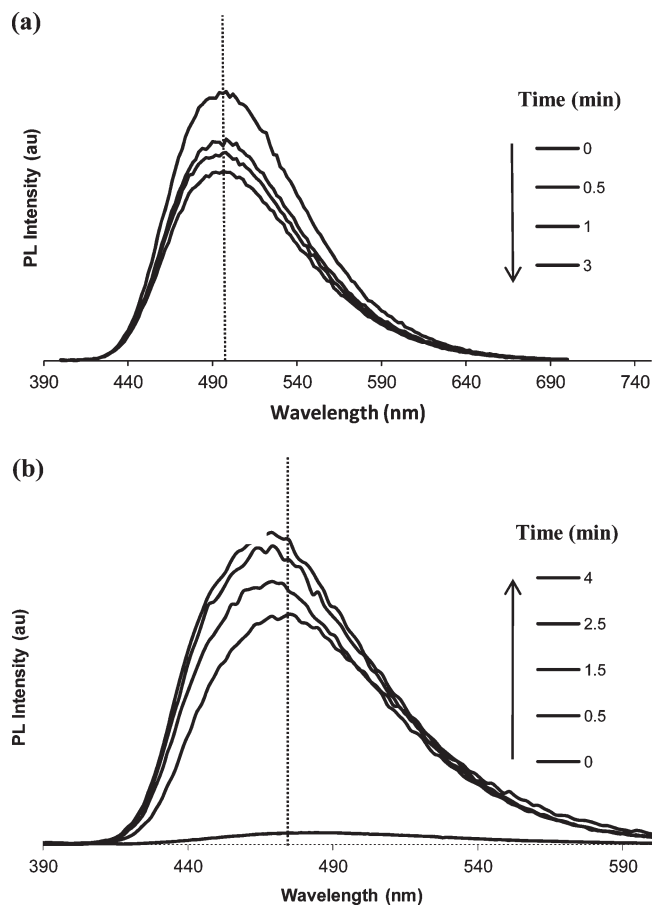


Figure 9. Spectra collected at different times depicting the effect of acetone vapor on **8** (a) and 1,1-diethynyl-2,3,4,5-tetraphenylgermole (b) coated on a quartz cell. Excitation at 375 and 365 nm, respectively.

representing the “OFF” switch. Once the acetone vapor evaporates, the emission resumes (Figure 8c), suggesting that the germole aggregates and, once again, emits light, representing the “ON” switch. This luminescence switch behavior was observed for all three of the germoles tested and can be repeated multiple times without diminishing the light emission.

In order to obtain a spectroscopic picture of how the photoluminescence changes upon exposure to VOCs, thin films of the germoles were exposed to the acetone vapor and monitored at regular time intervals using a spectrofluorimeter. The thin films were prepared by coating the inner wall of a quartz cell with ca. 10^{-3} M methylene chloride solutions of the germoles. A cotton swab tip saturated with acetone was placed in the bottom of the cell. A comparison of **8** with 1,1-diethynyl-2,3,4,5-tetraphenylgermole,²⁴ an AIE-active germole,^{9a,b} yielded an interesting result. Upon exposure to acetone vapor, light emission was rapidly quenched for both **8** and 1,1-diethynyl-2,3,4,5-tetraphenylgermole on TLC plates, but exhibited different luminescent behavior on quartz. The photoluminescence of the thin film of **8** on quartz decreased until the emission was practically quenched (Figure 9a), while the photoluminescence of 1,1-diethynyl-2,3,4,5-tetraphenylgermole blue-shifted and became stronger over time (Figure 9b).

Although this luminescent behavior appears contrary to the observed quenched emission on the TLC plate, a similar increase in photoluminescence on quartz was observed for hexaphenylsilole

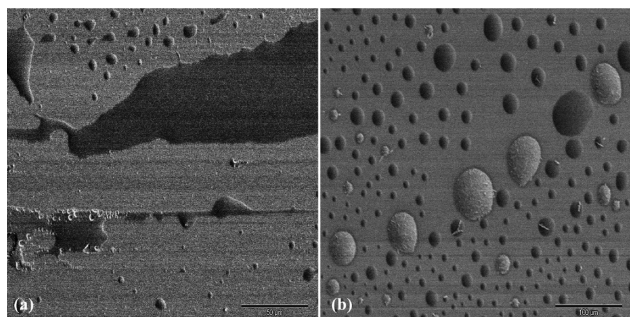


Figure 10. SEM images of the thin films of **8** (a) and 1,1-diethynyl-2,3,4,5-tetraphenylgermole (b), respectively, prior to exposure to acetone vapor using a lower E–T detector at 250 \times .

(HPS)²⁸ and 1,1-diethynyl-2,3,4,5-tetraphenylsilole.²⁵ SEM analysis of the quartz thin films conducted by Tang and co-workers revealed that the VOCs had induced crystallization in the supersaturated silole solution that formed as the vapor condensed on the thin film. The crystallization is thought to be the reason for the blue shift and enhanced emission, a hypothesis referred to as crystallization-enhanced emission (CEE).^{6a,b,25,28} According to the CEE effect, there are two types of aggregates in molecules that exhibit AIE, amorphous and crystalline, and the transformation from one form to another affects the photoluminescence. The difference between the two forms may lie in the degree of twisting of the peripheral aryl substituents. The conformation of amorphous aggregates was proposed to be slightly more planar than in crystalline aggregates, which lowered emission.^{6b} Using the CEE effect to explain the photoluminescence behavior observed in our experiment, it is probable that the acetone vapor condensed on the quartz thin film, forming a liquid layer containing the 1,1-diethynyl-2,3,4,5-tetraphenylgermole. In this liquid layer, the germole was not dissolved but instead rapidly transformed from an amorphous to crystalline form, resulting in the observed enhanced photoluminescence (Figure 9b). Since the photoluminescence of the thin film of **8** on quartz decreased (Figure 9a), then according to the CEE effect, the acetone vapor condensed on the quartz, forming a thin film that gradually dissolved the germole, which explains why the emission was quenched with prolonged exposure to the acetone vapor.

In order to further explore the CEE effect, the morphology of the quartz thin films of **8** and 1,1-diethynyl-2,3,4,5-tetraphenylgermole was investigated by SEM before and after exposure to acetone vapor. The high-resolution SEM images suggest that the thin films of **8** (Figure 10a) and 1,1-diethynyl-2,3,4,5-tetraphenylgermole (Figure 10b) are smooth and amorphous prior to exposure to acetone vapor. The images of the thin films after being exposed to acetone vapor for 10 hours suggest that acetone vapor induced both germoles to crystallize (Figure 11). Crystallization was observed for several of the other new germoles with minimal shifting of the emission wavelength maximum and diminished photoluminescence with prolonged exposure to acetone vapor.

Since this unique PL behavior for the thin films on quartz was only observed for hexaphenylsilole (HPS) and 1,1-diethynyl-2,3,4,5-tetraphenylsilole, Tang proposed that the highly symmetrical structures of these two siloles were able to pack more efficiently than unsymmetric siloles, which may have aided the crystallization process.²⁵ As a result of the efficient packing arrangement, multiple CH– π bonds were identified that were

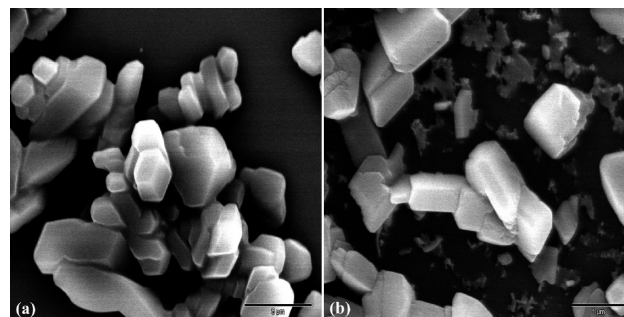


Figure 11. SEM images of the thin films of **8** (a) and 1,1-diethynyl-2,3,4,5-tetraphenylgermole (b) after 10 h exposure to acetone vapor using the higher E–T detector at 5000 \times and 20 000 \times , respectively.

speculated to further aid in restricting intramolecular motions of the aryl substituents by stiffening the conformation within the crystalline lattice, which enhanced the PL emission. The packing arrangement of the crystals of **8** was examined more closely for evidence of any cooperative bonding interactions. The crystal structure of **8** illustrates that adjacent molecules pack in such a way that the phenyl substituents are practically orthogonal and cannot overlap (Figure 12). The closest distance between the 3,4-phenyl substituents of two adjacent molecules of **8** is 6.9 Å (Figure 12a), which is too great a distance for any π – π stacking or CH– π interactions. The ring cores are staggered with respect to one another with an interplane distance between the germole cores of 10.5 Å (Figure 12b), too great a distance for any intermolecular interactions. There are, however, multiple CH groups as well as fluorine atoms present in **8** that may participate in nonconventional, weak CH– π hydrogen bonding in two regions within the packing arrangement. Both potential cooperative interactions involve the substituted phenyl ring of one of the 1,1-substituents with the phenyl substituents on an α -carbon in the ring core and another 1,1-substituent of a second molecule located directly above (Figure 12b). The distances between these segments are 3.0 and 2.7 Å, respectively. These measurements are within hydrogen-bonded and intermediate (type CH–X) intermolecular approaches of ca. 3.0 Å, which were demonstrated for edge-to-face orientations in several siloles.²⁹ Given the evidence of crystallization of **8** with prolonged exposure to acetone and the additional stabilizing effects of cooperative CH– π interactions, it is conceivable that the difference in photoluminescence on quartz between **8** and 1,1-diethynyl-2,3,4,5-tetraphenylgermole is the result of the time it takes for these new germoles to efficiently pack. The gradually diminishing PL of **8** on the quartz thin film implies that the condensing acetone vapor dissolved the germole. Once dissolved, the longer, bulkier 1,1-substituents on **8** experienced disorder and, therefore, required more time to properly orient and assemble so that crystallization and the ensuing cooperative CH– π interactions could occur. This could explain why the PL was not enhanced or blue-shifted within the time period that the quartz thin films were monitored using a spectrofluorimeter. It will be interesting to see if germoles in the crystalline phase are stronger, bluer emitters than their amorphous phase counterparts, as is the case for many AIE-active molecules.¹⁹ Efforts are currently underway to obtain absorption and emission data for the crystalline phase of the new germoles prepared in this report.

In conclusion, a series of new 2,3,4,5-tetraphenylgermole with different 1,1-substituents were synthesized and characterized. The new germoles intensely fluoresce in the blue-green

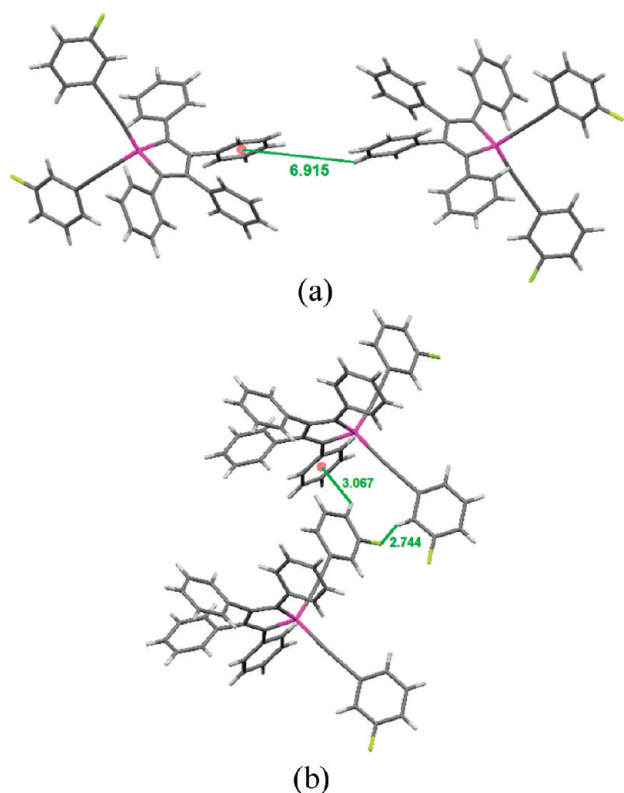


Figure 12. Packing arrangement of crystalline **8**, (a) showing the intermolecular distance between two molecules of **8** (6.9 Å) at the 3,4-diphenyl substituents; (b) showing the interplane separation between two molecules of **8** and the two shortest C–H– π hydrogen-bonding interactions of 3.0 and 2.7 Å.

region (478–488 nm) in the solid phase. The electronegativity of the 1,1-substituents exhibited a modest inductive effect on the UV–vis and fluorescence wavelength maxima. Although the new germoles exhibited higher quantum yields in solution than other characterized germoles, their room-temperature solutions are only weakly emissive. In comparison to siloles, the new germoles were ca. $3\times$ more emissive in solution, resulting in a smaller enhancement of luminescence when aggregated. The smaller enhancement between the luminescence of the molecularly dissolved and aggregated solutions of these germoles should not discourage exploiting the AIE effect in these systems. The AIE effect in the new germoles is quite pronounced and holds great promise for potential applications as efficient emitters in aqueous media. TEM analysis indicated the formation of crystalline nanoparticles in the mixed solvent–water systems, which aggregated into various sized clusters, resulting in enhanced PL and quantum yields. The AIE effect was utilized to investigate potential applications of the new germoles as chemosensors for VOCs. The photoluminescence on TLC plates exhibited reversible “on” and “off” switch behavior. By controlling the aggregation process, the light emission could be quenched in the presence of organic vapors, but resumed upon evaporation of the VOC.

EXPERIMENTAL SECTION

General Comments. All reactions were performed under an inert atmosphere of argon using flame- or oven-dried glassware on a dual-

manifold Schlenk line or in a drybox. Diethyl ether and THF were distilled over sodium/9-fluorenone prior to use. Methylene chloride was distilled over CaH_2 . Chloroform-*d* was purchased from Cambridge Isotopes Inc. and dried over activated molecular sieves. Other commercially available reagents were purchased from Aldrich Chemical Co. and were used as received. NMR spectra were recorded on Bruker Avance-300 MHz and Bruker ARX-500 MHz instruments at ambient temperature. Spectroscopic data were recorded at 300 and 500 MHz, respectively, for ^1H , 125 and 75 MHz respectively for ^{13}C , 202 MHz for ^{31}P , and 282 MHz for ^{19}F . Proton, carbon, phosphorus, and fluorine chemical shifts (δ) are reported relative to the residual protio- and deutero-chloroform, external H_3PO_4 , and CFCl_3 , respectively. Chemical shifts are reported in ppm and the coupling constants in hertz. Melting point determinations were obtained on a Mel-Temp melting point apparatus and are uncorrected. UV–vis and fluorescence spectra were measured on a Cary 50 Bio UV–visible and Cary Eclipse fluorescence spectrophotometer, respectively. Emission spectra were measured using the λ_{max} value for each compound as determined by the absorption spectra. Elemental analysis determinations were performed by Atlantic Micro-labs, Inc., Norcross, GA. The X-ray crystallographic data were collected on a Bruker Apex II diffractometer equipped with a CCD area detector.

For solid-state PL measurements, aluminum TLC plates (Merck, silica 60 F_{254}) were used. Dichloromethane solutions of the germoles (0.67 mg/mL) were used as the developing media. The coated TLC plates were excited at an angle of 20° in the spectrofluorometer. For dynamic light scattering measurements, the hydrodynamic radius (RH) was measured at room temperature with a DynaPro Titan instrument (Wyatt Technology, Santa Barbara, CA). Samples (30 μL) were placed directly into a quartz cuvette, and light scattering intensity was collected at a 90° angle using a 10 s acquisition time. Data regularization with Dynamics (version 6.7.1) generated histograms of percent mass versus RH.

For TEM images, a droplet of 0.05 mM acetone–water mixture was applied to a lacey carbon film on a square mesh copper grid (Ted Pella Inc.) and allowed to air-dry at 25°C . The aggregated samples were visualized with a Phillips EM 430 transmission electron microscope operated at 300 000 eV and magnifications of 110 000 and 150 000, respectively.

For SEM images, thin films were prepared by coating quartz slides with ca. 10^{-3} M methylene chloride solutions of the germoles. The morphologies were visualized with a JEOL-6320F field emission scanning electron microscope after sputtering a thin layer of gold onto the samples with a Hummer VI sputtering system. The operating parameters for the images taken with the lower detector were an acceleration voltage of 5 keV, probe current #3, objective lens aperture 3, and a working distance of 15 mm. The operating parameters for the higher detector were similar except that an acceleration voltage of 15 keV and a working distance of 8 mm were employed.

Representative Procedure. Formation of 1,1'-Bis(4-(trifluoromethyl)phenyl)-2,3,4,5-tetraphenylgermole (**2**). A solution of *n*-BuLi (0.50 mL, 2.5 M in hexane, 1.3 mmol) was added dropwise to a solution of 1-ethynyl-4-trifluorotoluene (0.20 mL, 1.3 mmol) in dry THF (1.5 mL) that had been cooled to -78°C . Once the addition was complete, the colorless reaction mixture was stirred at this temperature for 15 min. The resulting alkynyllithium solution was then added in one portion to a solution of 1,1'-dichloro-2,3,4,5-tetraphenylgermole (0.31 g, 0.63 mmol) in dry THF (5 mL) that had been cooled to 0°C . The yellow reaction mixture was allowed to gradually warm to room temperature and stirred overnight. The reaction mixture was quenched with water (0.25 mL), stirred for an additional 15 min, and then dried over MgSO_4 . After filtering, the solvent was removed by rotary evaporation. The crude product was purified on a silica gel column using toluene–hexane (2:1) as the eluent to give **2** as a yellow solid (340 mg, 71%). X-ray quality crystals were grown by slow evaporation from a methylene chloride–diethyl ether mixed-solvent system. All of

the other germoles were prepared in a similar manner. The eluent and recrystallization solvent systems used in the purification of each germole are indicated.

Formation of 1,1-Bis(4-(trifluoromethyl)phenyl)-2,3,4,5-tetraphenylgermole (2). Mp: 179–180 °C. ^1H NMR (500 MHz): δ 7.63 (d, J = 8 Hz, 4H), 7.57 (d, J = 8 Hz, 4H), 7.22 (d, J = 8 Hz, 4H), 7.16 (t, J = 8 Hz, 4H), 7.14–7.09 (m, 2H), 7.09–7.03 (m, 6H), 6.91–6.86 (m, 4H). $^{13}\text{C}\{^1\text{H}\}$ NMR (125 MHz): δ 153.5, 138.4, 137.7, 135.4, 132.7, 130.9 (q, J = 33 Hz), 129.85, 129.80, 128.2, 127.9, 127.0, 126.9, 126.2, 125.3 (q, J = 8 Hz), 124.9, 105.8, 88.6. $^{19}\text{F}\{^1\text{H}\}$ NMR (282 MHz): δ –62.9. Anal. Calcd for $\text{C}_{46}\text{H}_{28}\text{F}_6\text{Ge}$: C, 72.00; H, 3.68. Found: C, 71.74; H, 3.57.

Formation of 1,1-Bis(4-(trifluoromethoxy)phenyl)-2,3,4,5-tetraphenylgermole (3). Purification of **3** by column chromatography using silica gel and toluene–hexane (2:1) as the eluent yielded a yellow solid (461 mg, 67%). Mp: 113–114 °C. ^1H NMR (500 MHz): δ 7.61–7.57 (m, 4H), 7.28–7.25 (m, 4H), 7.22–7.17 (m, 8H), 7.17–7.14 (m, J = 5, 2 Hz, 2H), 7.13–7.07 (m, 6H), 6.94–6.90 (m, 4H). $^{13}\text{C}\{^1\text{H}\}$ NMR (125 MHz): δ 153.4, 149.6, 138.6, 137.8, 135.8, 134.1, 129.9, 129.8, 128.2, 127.9, 126.9, 126.8, 121.3, 120.9, 119.5, 105.8, 86.9. $^{19}\text{F}\{^1\text{H}\}$ NMR (282 MHz): δ –57.7. Anal. Calcd for $\text{C}_{46}\text{H}_{28}\text{F}_6\text{GeO}_2$: C, 69.12; H, 3.53. Found: C, 68.71; H, 3.59.

Formation of 1,1-Bis(*p*-tolylethynyl)-2,3,4,5-tetraphenylgermole (4). Purification of **4** by column chromatography using silica gel and hexane–toluene (2:1) as the eluent yielded a yellow solid (317 mg, 70%). Yellow crystals were grown by slow evaporation from a methylene chloride–hexane mixed-solvent system. Mp: 210.5–212 °C. ^1H NMR (500 MHz): δ 7.45 (d, J = 8 Hz, 4H), 7.31–7.27 (m, 5H), 7.20–7.12 (m, 10H), 7.11–7.05 (m, 6H), 6.94–6.90 (m, 4H), 2.38 (s, 6H). $^{13}\text{C}\{^1\text{H}\}$ NMR (125 MHz): δ 152.9, 139.4, 138.8, 138.1, 136.4, 132.4, 130.0, 129.8, 129.1, 128.1, 127.8, 126.7, 126.6, 119.6, 107.5, 85.2, 21.7. Anal. Calcd for $\text{C}_{46}\text{H}_{34}\text{Ge}$: C, 83.79; H, 5.20. Found: C, 83.46; H, 5.64.

Formation of 1,1-Bis(4-methoxyphenyl)ethynyl)-2,3,4,5-tetraphenylgermole (5). Purification of **5** by column chromatography using silica gel and toluene–hexane (2:1) as the eluent yielded a yellow solid (200 mg, 46%). Yellow crystals were grown by slow evaporation from a tetrahydrofuran–methanol mixed-solvent system. Mp: 250–252 °C. ^1H NMR (500 MHz): δ 7.48–7.43 (m, 4H), 7.24 (m, 4H), 7.14 (m, 4H), 7.11–7.06 (m, 2H), 7.06–7.01 (m, 6H), 6.90–6.86 (m, 4H), 6.84–6.80 (m, 4H), 3.79 (s, 6H). $^{13}\text{C}\{^1\text{H}\}$ NMR (125 MHz): δ 160.3, 152.8, 138.9, 138.2, 136.5, 134.0, 129.9, 129.8, 128.1, 127.8, 126.7, 126.5, 114.8, 113.9, 107.3, 84.4, 68.1, 55.4, 25.7. Anal. Calcd for $\text{C}_{46}\text{H}_{34}\text{GeO}_2$: One $\text{C}_4\text{H}_8\text{O}$: C, 78.65; H, 5.54. Found: C, 78.45; H, 5.42.

Formation of 1,1-Bis((1,1-biphenyl)-4-ylethynyl)-2,3,4,5-tetraphenylgermole (6). Purification of **6** by column chromatography using silica gel and hexane–toluene (2:1) as the eluent yielded a yellow solid (282 mg, 58%). Yellow crystals were grown by slow evaporation from a tetrahydrofuran–methanol mixed-solvent system. Mp: 186–188 °C. ^1H NMR (500 MHz): δ 7.63–7.53 (m, 12H), 7.47–7.41 (m, 4H), 7.38–7.34 (m, 2H), 7.29–7.27 (m, 4H), 7.19–7.14 (m, 4H), 7.13–7.09 (m, 2H), 7.08–7.03 (m, 6H), 6.93–6.87 (m, 4H). $^{13}\text{C}\{^1\text{H}\}$ NMR (125 MHz): δ 153.1, 141.9, 140.4, 138.8, 138.0, 136.2, 132.9, 129.98, 129.87, 129.0, 128.2, 127.92, 127.88, 127.2, 127.0, 126.8, 126.7, 121.5, 107.2, 86.7. Anal. Calcd for $\text{C}_{56}\text{H}_{38}\text{Ge}$: C, 85.84; H, 4.89; Found: C, 85.86; H, 4.82.

Formation of 1,1-Bis(4-phenoxyphenyl)ethynyl)-2,3,4,5-tetraphenylgermole (7). Purification of **7** by column chromatography using silica gel and hexane–toluene (2:1) as the eluent yielded a yellow solid (254 mg, 50%). Yellow crystals were grown by slow evaporation from a tetrahydrofuran–methanol mixed-solvent system. Mp: 204–205 °C. ^1H NMR (500 MHz): δ 7.54–7.49 (m, 4H), 7.42–7.36 (m, 4H), 7.30–7.25 (m, 4H), 7.20–7.15 (m, 6H), 7.14–7.10 (m, 2H), 7.10–7.07 (m, 6H), 7.06–7.02 (m, 4H), 6.96–6.92 (m, 4H), 6.92–6.89 (m, 4H). $^{13}\text{C}\{^1\text{H}\}$ NMR (125 MHz): δ 158.4, 156.4,

153.0, 138.8, 138.1, 136.3, 134.2, 130.1, 130.0, 129.8, 128.1, 127.9, 126.8, 126.6, 124.1, 119.7, 118.2, 117.1, 106.9, 85.2. Anal. Calcd for $\text{C}_{56}\text{H}_{38}\text{GeO}_2$: C, 82.47; H, 4.70. Found: C, 82.16; H, 4.82.

Formation of 1,1-Bis((3-fluorophenyl)ethynyl)-2,3,4,5-tetraphenylgermole (8). Purification of **8** by column chromatography using silica gel and hexane–toluene (2:1) as the eluent yielded a yellow solid (271 mg, 65%). Yellow crystals were grown by slow evaporation from a methylene chloride–hexane mixed-solvent system. Mp: 181.5–182.5 °C. ^1H NMR (500 MHz): δ 7.32–7.28 (m, 4H), 7.22 (m, 6H), 7.16 (m, 4H), 7.13–7.09 (m, 2H), 7.08–7.03 (m, 8H), 6.90–6.86 (m, 4H). $^{13}\text{C}\{^1\text{H}\}$ NMR (125 MHz): δ 162.4 (d, J = 247 Hz), 153.3, 138.6, 137.8, 135.7, 130.0 (d, J = 9 Hz), 129.9, 129.8, 128.3 (d, J = 3 Hz), 128.2, 127.9, 126.9, 126.8, 124.3 (d, J = 9 Hz), 119.2 (d, J = 23 Hz), 116.7 (d, J = 22 Hz), 105.9 (d, J = 3 Hz), 86.9. $^{19}\text{F}\{^1\text{H}\}$ NMR (282 MHz): δ –113.2. Anal. Calcd for $\text{C}_{44}\text{H}_{28}\text{F}_2\text{Ge}$: C, 79.19; H, 4.23. Found: C, 78.83; H, 4.00.

Formation of 1,1-Bis(thiophen-3-ylethynyl)-2,3,4,5-tetraphenylgermole (9). Purification of **9** by column chromatography using silica gel and hexane–toluene (2:1) as the eluent yielded a yellow solid (418 mg, 70%). Yellow crystals were grown by slow evaporation from a methylene chloride–hexane mixed-solvent system. Mp: 254–255.5 °C. ^1H NMR (500 MHz): δ 7.60 (d, J = 3 Hz, 2H), 7.28–7.24 (m, 6H), 7.22–7.14 (m, 6H), 7.14–7.10 (m, 2H), 7.10–7.05 (m, 6H), 6.93–6.88 (m, 4H). $^{13}\text{C}\{^1\text{H}\}$ NMR (125 MHz): δ 153.1, 138.8, 138.0, 136.1, 130.9, 130.4, 130.0, 129.9, 128.1, 127.9, 126.8, 126.7, 125.4, 121.9, 102.3, 85.6. Anal. Calcd for $\text{C}_{40}\text{H}_{26}\text{GeS}_2$: C, 74.67; H, 4.07. Found: C, 74.88; H, 3.97.

Formation of 1,1-Bis((3-pyridinyl)ethynyl)-2,3,4,5-tetraphenylgermole (10). Purification of **10** by column chromatography using silica gel and methanol as the eluent yielded a yellow solid (472 mg, 60%). Yellow crystals were grown by slow evaporation from a methylene chloride–diethyl ether mixed-solvent system. Mp: 220–221.5 °C. ^1H NMR (300 MHz): δ 8.76 (dd, J = 2, 0.7 Hz, 2H), 8.56 (dd, J = 5, 1.7 Hz, 2H), 7.81 (dt, J = 8, 1.9 Hz, 2H), 7.29–7.03 (m, 16H), 6.91–6.86 (m, 4H). $^{13}\text{C}\{^1\text{H}\}$ NMR (125 MHz): δ 153.5, 153.1, 149.5, 139.3, 138.5, 137.7, 135.5, 129.9, 129.8, 128.3, 128.0, 127.0, 126.9, 123.1, 119.7, 104.0, 89.7. Anal. Calcd for $\text{C}_{42}\text{H}_{28}\text{GeN}_2$: C, 79.65; H, 4.46. Found: C, 79.18; H, 4.36.

Formation of 1,1-Bis((2-pyridinyl)ethynyl)-2,3,4,5-tetraphenylgermole (11). Purification of **11** by column chromatography using silica gel and methanol as the eluent yielded a yellow solid (447 mg, 66%). Yellow crystals were grown by slow diffusion from a hexane–methylene chloride (2:1) mixed-solvent system. Mp: 260 °C (dec). ^1H NMR (300 MHz): δ 8.59 (ddd, J = 4.9, 1.7, 0.9 Hz, 2H), 7.66 (td, J = 7.7, 1.8 Hz, 2H), 7.54 (dt, J = 7.8, 1.1 Hz, 2H), 7.29–7.19 (m, 6H), 7.15–7.02 (m, 10H), 6.90–6.84 (m, 4H). $^{13}\text{C}\{^1\text{H}\}$ NMR (75 MHz): δ 153.8, 150.4, 142.9, 138.9, 137.9, 136.6, 135.7, 130.22, 130.15, 128.5, 128.4, 128.2, 127.1, 127.0, 124.0, 105.9, 86.6. Anal. Calcd for $\text{C}_{42}\text{H}_{28}\text{GeN}_2$: C, 79.65; H, 4.46. Found: C, 79.39; H, 4.91.

Formation of 1,1-Bis((diphenylphosphino)ethynyl)-2,3,4,5-tetraphenylgermole (12). Purification of **12** by column chromatography using silica gel and hexane–toluene (2:1) as the eluent yielded a yellow solid (450 mg, 44%). Yellow crystals were grown by slow evaporation from diethyl ether. Mp: 154.5–156 °C. ^1H NMR (500 MHz): δ 7.58–7.53 (m, 8H), 7.34–7.24 (m, 14H), 7.23–7.19 (m, 4H), 7.16–7.13 (m, 6H), 7.10–7.05 (m, 6H), 6.89 (dd, J = 8, 1.7 Hz, 4H). $^{13}\text{C}\{^1\text{H}\}$ NMR (125 MHz): δ 153.4, 138.5, 137.6, 135.7, 135.5 (d, J_{PC} = 6 Hz), 132.7 (d, J_{PC} = 21 Hz), 130.0, 129.9, 129.2, 128.8 (d, J_{PC} = 8 Hz), 128.2, 127.9, 126.9, 126.8, 107.2 (d, J_{PC} = 18 Hz), 106.5 (d, J_{PC} = 3 Hz). $^{31}\text{P}\{^1\text{H}\}$ NMR (202 MHz): δ –32.2. Anal. Calcd for $\text{C}_{56}\text{H}_{40}\text{GeP}_2$: C, 79.36; H, 4.76. Found: C, 79.69; H, 5.06.

X-ray Structure Determination. Crystals of X-ray diffraction quality were obtained by slow evaporation from a methylene chloride–hexane mixed-solvent system for **8** and a slow evaporation of a saturated diethyl ether solution for **12**. Crystals of appropriate dimension was mounted on a glass capillary in a random orientation. Preliminary

examination and data collection were performed using a Bruker Kappa Apex II charge coupled device (CCD) detector system single-crystal X-ray diffractometer using an Oxford Cryostream LT device. Data were collected using graphite-monochromated Mo K α radiation ($\lambda = 0.71073$ Å) from a fine focus sealed-tube X-ray source. Preliminary unit cell constants were evaluated with a set of 36 narrow frame scans. Typical data sets consist of combinations of φ scan frames with typical scan width of 0.5° and exposure time of 15–20 s/frame at a crystal to detector distance of 4.0 cm. The collected frames were integrated using an orientation matrix determined from the narrow frame scans. Apex II and SAINT software packages³⁰ were used for data collection and data integration. Final cell constants were determined by global refinement of reflections from the complete data set. Collected data were corrected for systematic errors using SADABS³⁰ based on the Laue symmetry using equivalent reflections.

Crystal data and intensity data collection parameters are listed in Table 1.

Structure solution for **8** was carried out using the SIR-92 software package,³¹ and structure refinement was performed using the CRYSTALS software package.³² Structure solution and refinement for **12** was performed using the SHELXTL 97 package.³⁰ The structures were solved by direct methods in the triclinic space group P1 and refined with full matrix least-squares refinement by minimizing $\Sigma w(F_o^2 - F_c^2)^2$. All non-hydrogen atoms were refined anisotropically to convergence. One of the phenyl rings in **12** is disordered over two positions. Disorder was resolved with 50% occupancy atoms. All H atoms were added in the calculated position and were refined using appropriate riding models. The models were refined to convergence to the final residual values of $R_1 = 4.0\%$ and $wR_2 = 11.2\%$ for **8** and $R_1 = 3.9\%$ and $wR_2 = 13.1\%$ for **12**. Complete listings of geometrical parameters, positional and isotropic displacement coefficients for hydrogen atoms, and anisotropic displacement coefficients for the non-hydrogen atoms are submitted as Supporting Information within the associated CIF files.

■ ASSOCIATED CONTENT

S Supporting Information. Expanded graph of the quantum yield versus water content for **2**, CIF files, crystal structures with labeled atoms and an abbreviated listing of the crystal data, structure solution and refinement, bond lengths and angles, and anisotropic displacement parameters for germales **2**, **4**, **5**, and **7–11**. This material is available free of charge via the Internet at <http://pubs.acs.org>.

■ AUTHOR INFORMATION

Corresponding Author

*E-mail: wilkingj@umsl.edu. Tel: +1-314-516-6436. Fax: 1-314-516-5342.

■ ACKNOWLEDGMENT

The authors would like to thank Dr. Michael R. Nichols in the Chemistry and Biochemistry Department for dynamic light scattering measurements, Dr. Nigam Rath for consultations concerning X-ray crystallography, Dr. Dan Zhou for training on the SEM, and David C. Osborn for the TEM measurements. Funding from the National Science Foundation is greatly appreciated (CHE-0719380) and MRI (CHE-0420497) for the Apex II diffractometer.

■ REFERENCES

- (1) Aubouy, L.; Huby, N.; Hirsch, L.; van der Lee, A.; Gerbier, P. *New J. Chem.* **2009**, *33*, 1290–1300.
- (2) Zhan, X.; Risko, C.; Amy, F.; Chan, C.; Zhao, W.; Barlow, S.; Kahn, A.; Bredas, J. L.; Marder, S. R. *J. Am. Chem. Soc.* **2005**, *127*, 9021–9029.
- (3) (a) Tamao, K.; Uchida, M.; Izumizawa, T.; Furukawa, K.; Yamaguchi, S. *J. Am. Chem. Soc.* **1996**, *118*, 11974–11975. (b) Yamaguchi, S.; Endo, T.; Uchida, M.; Izumizawa, T.; Furukawa, K.; Tamao, K. *Chem.—Eur. J.* **2000**, *6*, 1683–1692.
- (4) (a) Murata, H.; Malliaras, G. G.; Uchida, M.; Shen, Y.; Kafafi, Z. H. *Chem. Phys. Lett.* **2001**, *339*, 161–169. (b) Murata, H.; Kafafi, Z. H. *Appl. Phys. Lett.* **2002**, *80* (2), 189–191.
- (5) Kepler, R. G.; Beeson, P. M.; Jacobs, S. J.; Anderson, R. A.; Sinclair, M. B.; Valencia, V. S.; Cahill, P. A. *Appl. Phys. Lett.* **1995**, *66*, 3618–3620.
- (6) For selected reviews on AIE, see: (a) Lui, J.; Lam, J. W. Y.; Tang, B. Z. *J. Inorg. Organomet. Polym.* **2009**, *19*, 249–285. (b) Hong, Y.; Lam, J. W. Y.; Tang, B. Z. *Chem. Commun.* **2009**, 4332–4353. (c) Li, Z.; Dong, Y. Q.; Lam, J. W. Y.; Sun, J.; Qin, A.; Haubler, M.; Dong, Y. P.; Sung, H. H. Y.; Williams, I. D.; Kwok, H. S.; Tang, B. Z. *Adv. Funct. Mater.* **2009**, *19*, 905–917.
- (7) Yin, S.; Peng, Q.; Shuai, Z.; Fang, W.; Wang, Y.-H.; Luo, Y. *Phys. Rev. B* **2006**, *73*, 205409 (1–5).
- (8) Pagenkopf and co-workers were able to increase the emission intensities of several siloles in solution by manipulating the substituents at the 2,5-positions as well those directly attached to the silicon center. By increasing the steric bulk of the substituents at these positions, they were able to restrict intramolecular motions; this rigidity imparted by the restricted intramolecular motions increased the photoluminescence. For additional information refer to: Boydston, A. J.; Pagenkopf, B. L. *Angew. Chem., Int. Ed.* **2004**, *43*, 6336–6338.
- (9) For examples of AIE-active germales, see: (a) Law, C. C. W.; Chen, J.; Tang, B. Z. *Polym. Prepr.* **2003**, *44*, 929–930. (b) Law, C. C. W.; Chen, J.; Lam, J. W. Y.; Peng, H.; Tang, B. Z. *J. Inorg. Organomet. Polym.* **2004**, *14*, 39–51. (c) Mullin, J. L.; Tracy, H. J.; Ford, J. R.; Keenan, S. R.; Fridman, F. J. *Inorg. Organomet. Poly. Mater.* **2007**, *17*, 201–213. (d) Tracy, H. J.; Mullin, J. L.; Klooster, W. T.; Martin, J. A.; Haug, J.; Wallace, S.; Rudloe, I.; Watts, K. *Inorg. Chem.* **2005**, *44*, 2003–2011.
- (10) Dubac, J.; Laporterie, A.; Manuel, G. *Chem. Rev.* **1990**, *90*, 215–263.
- (11) Yamaguchi, S.; Itami, Y.; Tamao, K. *Organometallics* **1998**, *17*, 4910–4916.
- (12) Hissler, M.; Dyer, P. W.; Reau, R. *Coord. Chem. Rev.* **2003**, *244*, 1–44.
- (13) Curtis, M. D. *J. Am. Chem. Soc.* **1969**, *91*, 6011–6018.
- (14) Braye, E. H.; Hubel, W.; Caplie, I. *J. Am. Chem. Soc.* **1961**, *83*, 4406–4413.
- (15) Jones, A. C.; Sanders, A. W.; Bevan, M. J.; Reich, H. J. *J. Am. Chem. Soc.* **2007**, *129*, 3492–3493.
- (16) Huc, V.; Balueva, A.; Sebastian, R. M.; Caminade, A. M.; Majoral, J. P. *Synthesis* **2000**, 726–730.
- (17) Cambridge Structural Database (CSD version 5.32) search performed on 02/24/2011.
- (18) Chen, J.; Law, C. C. W.; Lam, J. W. Y.; Dong, Y.; Lo, S. M. F.; Williams, I. D.; Zhu, D.; Tang, B. Z. *Chem. Mater.* **2003**, *15*, 1535–1546.
- (19) Lui, J.; Lam, J. W. Y.; Tang, B. Z. *J. Inorg. Organomet. Polym.* **2009**, *19*, 249–285.
- (20) Zhan, X.; Barlow, S.; Marder, S. R. *Chem. Commun.* **2009**, 1948–1955.
- (21) Yamaguchi, S.; Jin, R. Z.; Tamao, K. *J. Organomet. Chem.* **1998**, *559*, 73–80.
- (22) Chen, J.; Law, C. C. W.; Lam, J. W. Y.; Dong, Y.; Lo, S. M. F.; Williams, I. D.; Zhu, D.; Tang, B. Z. *Chem. Mater.* **2003**, *15*, 1535–1546.
- (23) Tong, H.; Hong, Y.; Dong, Y.; Haussler, M.; Li, Z.; Lam, J. W. Y.; Dong, Y.; Sung, H. H. Y.; Williams, I. D.; Tang, B. Z. *J. Phys. Chem. B* **2007**, *111*, 11817–11823.
- (24) Brocks-Meier, F.; Weiss, E. *J. Organomet. Chem.* **1993**, *453*, 33–45.

- (25) Dong, Y.; Lam, J. W. Y.; Qin, A.; Li, Z.; Sun, J.; Dong, Y.; Tang, B. Z. *J. Inorg. Organomet. Polym.* **2007**, *17*, 673–678.
- (26) Hamai, S.; Hirayama, F. *J. Phys. Chem.* **1983**, *87*, 83–89.
- (27) (a) Sanekata, M.; Suzuka, I. *Chem. Phys. Lett.* **2000**, 323, 98–104. (b) Chen, W.; Cai, W.; Wang, G.; Zhang, L. *Appl. Surf. Sci.* **2001**, *174*, 51–54.
- (28) Dong, Y.; Lam, J. W. Y.; Li, Z.; Qin, A.; Tong, H.; Dong, Y.; Feng, X.; Tang, B. Z. *J. Inorg. Organomet. Polym. Mater.* **2005**, *15*, 287–291.
- (29) Karle, I. L.; Butcher, J.; Wolak, M. A.; da Silva Filho, D.; Uchida, M.; Bredas, J.; Kafafi, Z. A. *J. Phys. Chem. C* **2007**, *111*, 9543–9547.
- (30) SADABS; Bruker Analytical X-Ray; Madison, WI, 2008.
- (31) Altomare, A.; Cascarano, G.; Giacovazzo, C.; Guagliardi, A.; Burla, M. C.; Polidori, G.; Camalli, M. *J. Appl. Crystallogr.* **1994**, *27*, 435.
- (32) Betteridge, P. W.; Carruthers, J. R.; Cooper, R. I.; Prout, K.; Watkin, D. J. *J. Appl. Crystallogr.* **2003**, *36*, 1487.